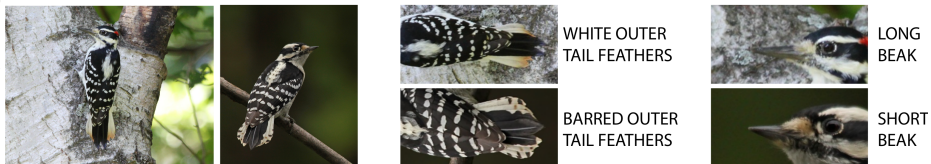


# Fine-grained Visual Categorization using PAIRS: Pose and Appearance Integration for Recognizing Subcategories

Pei Guo, Ryan Farrell

Brigham Young University

**Abstract.** Fine-grained Visual Categorization (FGVC) saw a tremendous boost between 2013 and 2016 with the incorporation of deep learning, however, progress has recently begun to slow. In this work, we postulate that one key to continued advances in fine-grained recognition performance is a better, and specifically, a more explicit, understanding of pose and appearance. We propose a model that predicts an object’s pose and then describes its appearance relative to the estimated pose. Our representation leveraging pose-aligned appearance patches was evaluated on and achieves state-of-the art performance for two key fine-grained datasets, CUB-200 and NABirds, most notably raising the standard for the widely-used CUB-200 dataset by nearly 2% to 89.2%.



**Fig. 1. Pose-aligned Patch Example.** The two woodpeckers shown on the left are distinct species (Hairy Woodpecker, Downy Woodpecker), yet they appear nearly identical. Because these foreground objects are so similar, a classification algorithm will likely search for discriminative features in the background. Alternately using an appearance representation based on *pose-aligned patches* like those shown on the right highlights differences between the two species – like the barring on the outer tail feathers or the far shorter beak length relative to the eye size.

## 1 Introduction

Fine-grained visual categorization (FGVC), also known as fine-grained recognition, refers to the task of taking a group of objects in a common, basic-level category, and classifying each object into one of many subordinate or “fine-grained” categories. Examples include distinguishing bird species [1,2,3] such as California Gull and Western Gull; discriminating between dog breeds [4,5,6] such as Golden Retriever and Labrador

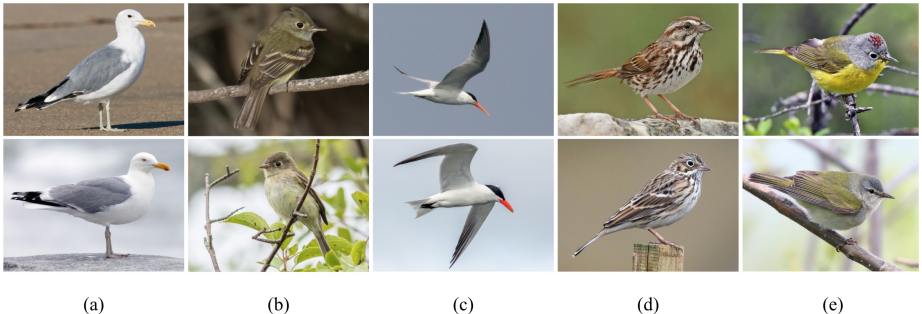


**Fig. 2. Examples of visually similar species.** Each column shows two visually similar species with subtle but key differences. (a): California Gull (dark eye and yellow leg) and Herring Gull (pale eye and pink leg). (b): Acadian Flycatcher and Least Flycatcher (smaller beak). (c): Elegant Tern (Thin and pink bill) and Caspian Tern (Thick and reddish bill). (d): Song Sparrow (thick eyebrow and malar stripes) and Vesper Sparrow (white eyering). (e): Nashville Warbler (pale eyeline and yellow belly) and Tennessee Warbler (dark eyeline and whitish belly).

Retriever; and differentiating between car makes and models [7,8] such as Toyota Prius and Honda Insight.

FGVC can be extremely difficult because categories are often very similar. Sometimes the only cues available to visually separate such species lie in highly-localized patches. Examples of visually similar categories and their key differences can be found in Figure 2. An ideal fine-grained recognition method would be able to recognize any image of any species.

With the emergence of deep learning [9], fine-grained recognition initially saw dramatic increases in accuracy. Building on deep learning architectures, recent approaches have typically either (i) looked at an object globally (*e.g.* [10,11,12]) or (ii) used an attention mechanism to focus on particular regions (*e.g.* [13,14,15,16]). Both paradigms have disadvantages. Looking at objects globally has little hope of finding the subtle highly-localized differences that, depending on the object’s pose and the camera’s viewing angle, can appear anywhere in the image. Attention, on the other hand, helps focus on a small number of regions but has little explicit notion of pose. Moreover, training data is often limited in the long-tailed distributions seen in many fine-grained domains. In such cases, both techniques suffer as the scarce training imagery does not adequately span the space of pose and viewing angle for each category, hindering their ability to recognize *any* species in *any* pose.

Improvements in the state-of-the-art, however, have slowed in recent years (Figure 3). We postulate that this may, in large part, be due to models that lack a sufficiently deep understanding of object pose and its subsequent influence on the object’s appearance in an image. A very promising direction is therefore to pursue a representation that incorporates a deeper understanding of pose, thus enabling a richer pose-aligned characterization appearance. Toward this end, we propose a novel fine-grained recognition algorithm called PAIRS (Pose and Apppearance Integration for Recognizing Subcategories). The PAIRS algorithm has four stages: (i) a highly-effective keypoint-

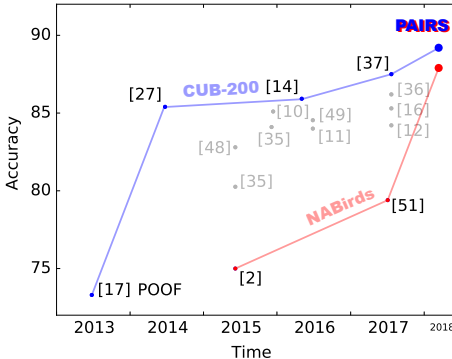


**Fig. 3. Progress over time on the CUB-200-2011 [1] and NABirds [2] datasets.** After rapid progress with the advent of deep learning, progress has slowed in recent years. We believe that this is due in part to a shallow, implicit understanding of object pose. The explicitly pose-aligned appearance representation we propose in the PAIRS framework constitutes renewed progress and achieves state-of-the-art performance, raising the bar by nearly 2% for the CUB-200 dataset to 89.2% and the best mark on the NABirds dataset by more than 8% to a new high of 87.9%. Grey points represent results on CUB that approached but were not state-of-the-art at their respective time of publication.

based pose-estimation network; (ii) pose-aligned patch extraction; (iii) per-patch feature extraction and classification; and (iv) a patch aggregation network for the final classification. Part annotations are only needed during the training phrase.

The trend in recent work using part-attention mechanisms [13,14,15,16] focuses on combining localization of *axis-aligned* rectangular regions with classification of those regions’ content in an end-to-end architecture. Our work demonstrates, however, that the ability to accurately recognize subcategories is less dependent on end-to-end than it is on the underlying appearance representation. A design that characterizes appearance relative to *pairs* of keypoints (first proposed in POOF [17]) affords the creation of an overcomplete basis of *pose-aligned* patches, ultimately providing the PAIRS framework with superior discriminative power. The proposed algorithm leverages the pose-aligned representation to achieve significant improvements over the state of the art on two challenging fine-grained datasets, CUB-200-2011 [1] and NABirds [2]. Most notably, on the widely-used CUB-200 dataset, a nearly 2% improvement is realized over the previous state-of-the-art method (see Figure 3).

## 2 Background and Related Work

Fine-grained visual categorization (FGVC) lies between generic category-level object recognition like the VOC [18], ImageNet [19], COCO [20], *etc.* and instance-level classification like facial recognition and other visual biometrics. The challenges of FGVC are many-fold: differences between similar species are often subtle and highly-localized and thus difficult even for (non-expert) humans to identify. Dramatic pose changes in-

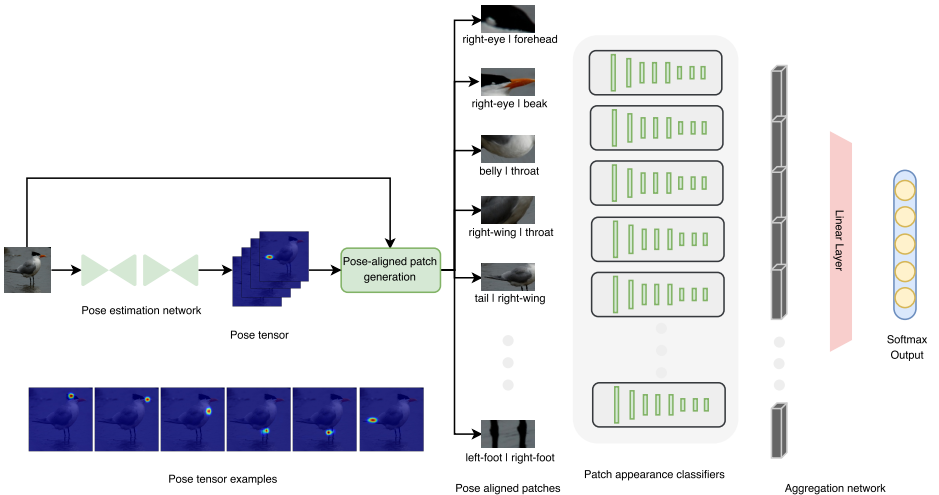


**Fig. 4. Overview of the Proposed Framework for Fine-grained Recognition.** We first apply a pose estimation network to the image for keypoint detection. Pose-aligned patches are then extracted from the image using the predicted keypoint locations. We then do fine-grained prediction on the individual patches using patch specific networks. These per-patch predictions are concatenated and fed into an aggregation network for the final fine-grained classification.

introduce great intra-class variance. Generalization also becomes an issue as the network struggles to find truly useful and discriminative features.

FGVC has caused wide attention in the computer vision community. Some early works include [21,22,5,23,24,25,26]. Birdlet, a volumetric poselet representation is proposed to account for the pose and appearance variation in [22]. [26] further proposes two pose-normalized descriptors based on computationally-efficient deformable part models. Although these early works seek to integrate pose and appearance like our method does, they rely heavily on hand-engineered descriptors thus have limited success on classification accuracy.

Our work is closely related to part-based CNN models [27,13,28,29,14,30], which seek to decompose the object into semantic parts. [29] first employs an object detection framework – R-CNN [31] for object and part detection. Part-Stacked CNN [32] proposes a fully convolutional network for keypoint detection and a two-stream convolutional network for object and part level feature extraction. Deep LAC [30] proposes a valve linkage function for back-propagation chaining and form a deep localization, alignment and classification system. [14] introduces an end-to-end learning framework for joint learning of pose estimation, normalization and recognition. These models are all based on a limited number of single keypoint patches, which could be poorly-aligned in the presence of pose and viewpoint variance.

There are also works targeting the object alignment problem. Unlike previous methods which rely on detectors for part localization, [33,34] proposes to localize distinctive details by roughly aligning the objects using just the overall shape. Spatial transformer

network [35] introduces a differentiable affine transformation learning layer to transform and align the object or part of interest.

Another direction in fine grained recognition is feature correlation and kernel mapping. [10] proposes a bilinear pooling layer to compute a second order polynomial kernel mapping on CNN features. Many works has followed this simple paradigm [11,12,36]. Compact bilinear pooling [11] proposes a compact representation to approximate the polynomial kernel, reducing memory usage. Low-rank bilinear pooling [12] represents the covariance features as a matrix and applies a low-rank bilinear classifier. Kernel pooling [36] proposes a general pooling framework that captures higher order interactions of features in the form of kernels. This line of works achieves relatively good results with weakly supervision, however, they attend to the whole image globally, lacking part-level information discovery mechanism. This limites their success in further accuracy improvement.

Inspired by human attention mechanism, many attempts have been made to guide the attention of the CNN model to informative object parts. Works along this direction include [16,37,38,39,40,41]. [42] proposes a multi-attention convolutional neural network (MA-CNN), where part generation and feature learning can reinforce each other. [37] leverages long short term memory networks (LSTM) to unify new patch candidates generation and informative part evaluation. This work establishes the current state-of-the-art performance on CUB-200-2011 [1] dataset, achieving an accuracy of 87.5% with part annotations. The key difference is our PAIRS representation integrates pose and appearance information and achieves multi-level attention over semantic object parts explicitly at the same time.

We note that Krause, *et al.* [43] achieved the highest accuracy on the CUB dataset at 92.3%. However, few works consider or include this work in comparisons because their model was trained on more than 4.8 million noisily-labeled images outside of the canonical CUB dataset.

### 3 PAIRS - Pose and Appearance Integration

We illustrate our algorithm pipeline in Figure 4. Firstly, we propose a simple yet effective fully convolutional neural network modified from a pretrained classification model for pose estimation (Figure 5). We follow the prevailing modular design paradigm by stacking convolutional blocks with the same topology. we show our pose estimation network achieves supreme results on the CUB-200 dataset both qualitatively and quantitatively. Secondly, given detected keypoint locations, a rectangle bounding box enclosing each keypoint pair is cropped from the original image and similarity-transformed to a uniform-sized patch (Figure 6), such that both keypoints are at fixed position across different images. As the representation is normalized to the keypoint locations, the patches are well-aligned, independent of the pose or the viewer’s angle. Thirdly, we train separate CNN models as initial patch classifiers for the pose-aligned patch representation. Lastly, we explore different architectures to aggregate the patch scores based on the assumption that part contribution should vary for different images and classes. We find surprisingly that the Multi-Layer Perception (MLP), while being the most simple method, achieves the best final classification accuracy.

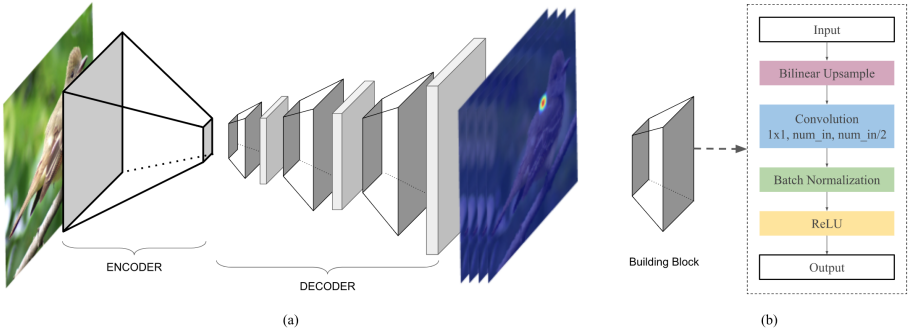


**Fig. 5. Pose Estimation Network.** We show the architecture of the proposed fully convolutional network for pose estimation in (a). The encoder part is a composed of a base CNN model such as VGG or ResNet. The decoder part is composed of stacked building blocks, each block formed by the sequence of layers shown in (b). Efforts to improve the architecture such as additional convolutional layers or learnable transposed convolutional upsampling layers achieves limited success, so we retain the architecture shown. This model yields the best reported results on the CUB-200 dataset.

### 3.1 Pose Estimation Network

Pose estimation networks usually follow one of two paradigms for prediction. The first is to directly regress discrete keypoint coordinates, e.g.  $(x_i, y_i)$ . Representative approaches include [44]. The alternate approach [45] instead uses a two-dimensional probability distribution heat map to represent the keypoint location. We call this resulting multi-channel probability distribution matrix *pose tensor*.

In this paper, we adopt the second strategy, proposing a fully convolutional network to produce the structured output distribution (Figure 5). Specifically, we take a pretrained classification network and remove the final classifier layer(s), retaining what can be seen as an encoder network that encodes strong visual semantics. We follow the prevailing modular design to stack repeated building blocks to the end of the network. The resulting block consists of one upsampling layer, one convolutional layer, one batch normalization layer and one ReLU non-linearity layer. The parameter-free bilinear interpolation layer is used for upsampling. The convolutional layer has 1x1 kernel and reduces the input channel size to half. Additionally, a final convolutional layer and upsampling layer are added to produce the pose tensor. There are many modifications one can make to enhance this basic model, including using larger 3x3 kernels, adding more convolutional layers to the building block, adding residue connection to each block, stacking more building blocks, and using a learnable transposed convolutional layer for upsampling. We find these structures provide only limited improvement but introduce more parameters, so we prefer this simpler architecture.

### 3.2 Patch Generation

Historically, part-based representations would model parts either as rectangular regions [29,46] or keypoints. Keypoints are convenient for pose-estimation. However,

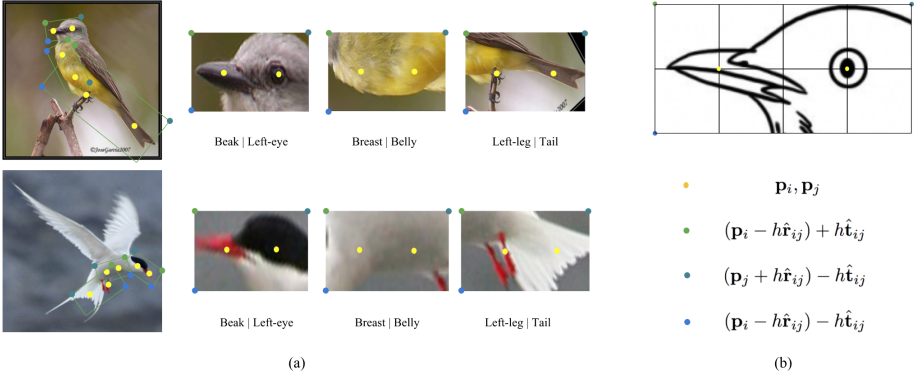


**Fig. 6. Pose-aligned Patch Generation.** We show the pose-aligned patch generation in this graph. For each pair of keypoints, we fit a rectangle bounding box whose corners are calculated as in (b). Objects of different poses and from different viewpoint can be compared directly by the proposed keypoint pair patch as shown in (a). Details are described in Section 3.2.

the square or rectangular patches, each centered on a given keypoint and extracted to characterize the part’s appearance, are far from optimal in the presence of rotation or general pose variation. We instead, propose to use keypoint pairs as anchor points in extracting pose-aligned patches.

Given two keypoints  $\mathbf{p}_i = (x_i, y_i)$  and  $\mathbf{p}_j = (x_j, y_j)$ , we define the vectors  $\mathbf{r}_{ij} = \mathbf{p}_j - \mathbf{p}_i$ , and  $\hat{\mathbf{r}}_{ij} = \mathbf{r}_{ij}/\|\mathbf{r}_{ij}\|_2$ . We also define the vector  $\hat{\mathbf{t}}_{ij} = \hat{\mathbf{z}} \times \hat{\mathbf{r}}_{ij}$ , a unit vector perpendicular to  $\mathbf{r}_{ij}$ , and the distances  $d = \|\mathbf{r}_{ij}\|_2$  and  $h = d/2$  for convenience. We seek to extract a region around  $\mathbf{p}_i$  and  $\mathbf{p}_j$  that is aligned with  $\mathbf{r}_{ij}$  and has dimensions  $2d \times d$ . The four corners of this rectangular region are then given by:

$$\begin{bmatrix} (\mathbf{p}_i - h\hat{\mathbf{r}}_{ij}) + h\hat{\mathbf{t}}_{ij} & (\mathbf{p}_j + h\hat{\mathbf{r}}_{ij}) - h\hat{\mathbf{t}}_{ij} \\ (\mathbf{p}_i - h\hat{\mathbf{r}}_{ij}) - h\hat{\mathbf{t}}_{ij} & (\mathbf{p}_j + h\hat{\mathbf{r}}_{ij}) + h\hat{\mathbf{t}}_{ij} \end{bmatrix} \quad (1)$$

A similarity-transform is computed to extract the pose-normalized patch. Patches generated in this way contain stable pose-aligned features – features near these keypoints appear at the same location in the given patch different images independent of the object’s pose or the camera viewing angle.

### 3.3 Patch Feature Extraction

A separate patch classification network is trained for each posed-aligned  $A \mid B$  patch. The softmax output from each network are concatenated as the representation for the input image. Alternatively, the final convolutional layer output after pooling can also be used and the result is comparable. We find that symmetric parts can help reduce the overall classifier number by nearly 50%, which is described in Section 4.2. The proposed patch representation can be seen as spatial pyramid that explicitly captures information of different parts at multiple spatial scales on the object (Figure 6).

### 3.4 Patch Aggregation Network

To fully utilize the abundant patch representations, we explore different ways to form a strong aggregation network. Based on the assumption that only a small fraction of the patches contains discriminative information and patches contribution should be weighted, we explores the following strategies.

- 1). **Fixed patch selection**: take the average score for a fixed number of top ranking patches. This strategy can also predicts the potential of our PAIRS representation.
- 2). **Dynamic patch selection**: employ the sparsely gated network [47] to dynamically learn a selection function to select a fixed number of patches for each input.
- 3). **Sequential patch weighting**: apply a Long Short Term Memory Networks (LSTM) to reweigh different patch features in a sequential way.
- 4). **Static patch weighting**: learn a Multi-Layer Perceptron network, which essentially applies a non-linear weighting function to aggregate information from different patches.

We find surprisingly that the MLP network, while being the simplest network architecture, achieves the best accuracy out of all the attempts we made. Details are included in the experiment section.

**Table 1. PCK comparison**

	back	beak	belly	breast	crown	forehead	left-eye	left-leg
[13]	80.7	89.4	79.4	79.9	89.4	88.5	85.0	75.0
[14]	85.6	94.9	81.9	84.5	94.8	96.0	95.7	64.6
Ours	<b>91.3</b>	<b>96.8</b>	<b>89.0</b>	<b>91.5</b>	<b>96.9</b>	<b>97.6</b>	<b>96.9</b>	<b>80.2</b>
	left-wing	nape	right-eye	right-leg	right-wing	tail	throat	<b>Overall</b>
[13]	67.0	85.7	86.1	77.5	67.8	76.0	90.8	86.6
[14]	67.8	90.7	93.8	64.9	69.3	74.7	94.5	N/A
Ours	<b>76.8</b>	<b>94.6</b>	<b>97.4</b>	<b>80.3</b>	<b>75.3</b>	<b>83.6</b>	<b>97.4</b>	<b>90.5</b>

## 4 Experimental Evaluation

We test our algorithm on two datasets, the CUB-200-2011 dataset and the NABirds dataset. The CUB-200-2011 contains 200 species of birds with 5994 training images and 5794 testing images. The NABirds dataset has 555 common species of birds in North America with a total number of 48,562 images. Class labels and keypoint locations are provided in both datasets.

### 4.1 Keypoint prediction performance

We use PCK (Percentage of Correct Keypoints) score to measure the accuracy of keypoint prediction results. A predicted keypoint ( $p$ ) is “correct” if its within a small neigh-



**Fig. 7. Keypoint localization results** We show the keypoint detection results of our fully convolutional pose estimation network. Red dots represent the predicted location and black dots are the ground truth locations. Our algorithm achieves high-level robustness over various scale and pose variation.

borhood of the ground truth location ( $g$ ), or equally speaking,

$$\|p - g\|_2 \leq c * \max(h, w)$$

$c$  is a constant factor and  $\max(h, w)$  is the longer side of the bounding box.

We evaluate our pose estimation network on CUB-200 and compare our PCK score with the others in Table 1. We achieve highest score on all 15 keypoints with considerable leading margin. We do especially well on legs and wings where other models struggle to make precise prediction. Some visualization results are shown in 4.1

Although we localize wings and legs better than baselines, they still have the lowest PCK in our model. This is caused by dramatic pose change as well as the appearance similarity between symmetric parts. We note that using keypoints to denote the wings isn't always appropriate. Because wings are two dimensional planar parts that spread over a relatively large area. Designating a keypoint to the wing can be obscure, because it is not easy to decide which point represents the wing location better. In fact, the ground truth keypoint location of the CUB dataset is the average of five annotators' results and it's even hard for them to reach a consensus.

## 4.2 Patch Classification Network

We adopt the ResNet-50 architecture as the patch classification network due to its high performance and compact GPU footprint. Alternate architectures like VGG and Inception can easily be adapted. We now discuss two considerations which facilitate training the patch classification network.

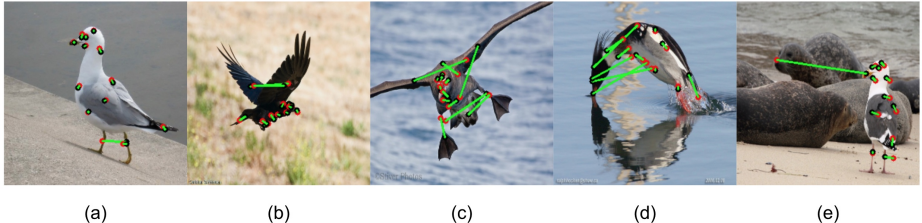


**Fig. 8. Keypoint localization failure patterns.** Three failure patterns are shown here. (a) and (b) confuse left and right because of the visual similarity between symmetric parts. Dramatic and rare pose causes degradation for keypoint localization as seen in (c) and (d). (e) shows an interesting case where the nose of a seal is mistakenly predicted as the gull’s beak. This reveals heavily cluttered background can hurt performance.

**Symmetry.** For a given object with  $n$  keypoints, the total number of patches to be classified is:

$$\binom{n}{2} = \frac{n(n-1)}{2} = \mathcal{O}(n^2)$$

which increases quadratically with  $n$ . Most real world objects show some kind of symmetry. Due to the visual similarity inherent in symmetric pairs keypoints (for example, right and left eyes, wings and feet), we treat each pair as a hybrid keypoint in the patch generation process. Many real-world objects, however, like birds, cats, cars, *etc.* are symmetric in appearance. Based on this observation, we propose to merge the patches for a symmetric pair of keypoints into a hybrid patch, *e.g.* left-eye | tail and right-eye | tail can be merged into the hybrid eye | tail pair. As a result, the total number of patch classification networks is reduced from 105 to 69 for the CUB dataset; on the NABirds dataset, the number is reduced from 55 to 37.

**Visibility.** Due to self-occlusion or foreground-occlusion, not all keypoints are visible in the image. Previous works [13] would eliminate patches with invisible keypoints to purify the input data. Contrarily, we find that this would hurt the performance of the patch classifiers. Details for comparison can be found in Figure 9. We believe this degradation is caused by the shrinkage of effective training set size. This is a similar finding with [43] that noisy but abundant data consistently outperforms clean but limited-sized data. Additionally, the pose estimation network would make a reasonable guess even if the keypoint is invisible. So during patch classifier training, all keypoints are considered visible by taking the maximally activated location.

### 4.3 Aggregation Network

Based on the assumption that image patches should contribute differently to classification. Four different strategies are explored and we describe details of them in this section.

**Fixed patch selection.** We assume only few patches contains useful information and others may merely act as noise. We propose a fixed patch selection strategy to keep the

best  $k$  patches. A greedy search algorithm would evaluate each  $n$  choose  $k$  combinations for  $k$  from 1 to  $n$ . The number of evaluations needed for this algorithm is

$$\sum_{k=1}^n \binom{n}{k} = \sum_{k=1}^n \frac{n!}{k!(n-k)!} = \mathcal{O}(n!)$$

The complexity grows in the order of  $n!$  and quickly becomes intractable. We thus employ the *beam search* algorithm. Instead of greedily searching the whole parameter space, we only keep a fixed  $k$  combinations each iteration and build our search path based only on previously learned  $k$  patch combinations. Out of curiosity, we also do beam search on the testing set alone. This operation, although invalid, provides some insights in the potential of our pose aligned patch representation. The results are shown in Figure 9. Our observations is that without overfitting, the potential of fixed patch selection should be well above 89%, compared to the current state-of-the-art [37] 87.5%. Notably, a simple average over all strategy can achieve 87.6%.

**Dynamic patch selection.** As an alternative attempt we experiment with is the sparsely gated network [47] for dynamic patch selection. Different from the beam search algorithm which selects fixed patches for each input, the gated network would select different combinations depending on the input. A tiny network is trained to predict weights for each patch and an explicit sparsity constraint is exposed on the weight to only allow  $k$  non-zero elements. A Sigmoid layer is added to normalize the weight. The network architecture can be described as,

$$G(x) = \text{softmax}(\text{top\_k}(H(x)))$$

$H(x)$  represents the mapping function from the input to patch weight.  $G(x)$  is the patch selection function. Different architectures for the tiny network are tried and we find a simple linear layer would work decently most of the time. Best accuracy is achieved when  $k = 105$ . Interestingly when  $k=1$ , our dynamic patch selection performs worse than the fixed patch selection, implying the gated network's inability to learn useful information for decision making.

**Sequential patch weighting.** Recurrent neural networks (RNN) is specialized at processing sequential data like text and speech. RNN has been widely adopted as an attention mechanism to focus on different parts sequentially. We instead employ RNN for sequential patch weighting, aiming to discover different patches for decision making. We employ a one-layer Long Short Term Memory (LSTM) network with 512 nodes. Each node has a hidden layer of size 1024. The last output of sequence is selected as the final output. We get 82.7% in this experiment and this confirms the effectiveness of the LSTM network.

**Static patch weighting** The final and most effective method we tried is the MLP network. The MLP network contains one hidden layer with 1024 parameters, followed by the batch normalization layer, ReLU layer, and then the output layer. On CUB our final accuracy is 88.7% , 1.2% higher than the current state-of-the-art result. We combine pairs patch with single keypoint patch and achieves a new state-of-the-art 89.2% accuracy. We compare our result with several other strong baselines in Table- 2.

We test our algorithm also on the NAbirds dataset and the result is shown in 3. Our algorithm attains an accuracy of 87.9%, more than 8% better than a strong baseline.

**Table 2. Classification score on CUB.** Annotation key as follows: GT = class labels; BB = bounding box annotation; KP = keypoint annotations; WEB = images downloaded from the Internet.

	Annotations	Accuracy
Huang <i>et al.</i> [13]	GT+BB+KP	76.2
Zhang <i>et al.</i> [29]	GT + BB	76.4
Krause <i>et al.</i> [48]	GT+BB	82.8
Jaderberg <i>et al.</i> [35]	GT	84.1
Shu <i>et al.</i> [12]	GT	84.2
Zhang <i>et al.</i> [49]	GT	84.5
Xu <i>et al.</i> [50]	GT+BB+KP+WEB	84.6
Lin <i>et al.</i> [10]	GT+BB	85.1
Cui <i>et al.</i> [36]	GT	86.2
Lam <i>et al.</i> [37]	GT+KP	87.5
PAIRS Only	GT + KP	88.7
PAIRS+Single	GT + KP	<b>89.2</b>

**Table 3.** Performance Comparison on the NABirds dataset.

Algorithm	Accuracy
ResNet-50 Baseline	79.2%
Bilinear CNN (PAMI 2017) [51]	79.4%
<b>PAIRS</b>	<b>87.9%</b>

#### 4.4 Results Visualization

We show the patch classification accuracy for each patch in the CUB dataset in Figure 9. The best performing patch corresponds to `belly` | `crown`, achieving 79.6% accuracy. The worst performing patch is the `left-leg` | `right-leg` pair which achieves only 15.7% accuracy. Empirically, global patches perform better than local patches, however local patches are also important for localizing discriminative object parts. Patches found by beam search, as shown in Figure 9, can provide insight – a combination of global and local patches are selected to achieve an optimal result.

As hard cases often can only be classified by a few highly localized discriminative parts, the number of patches with correct predictions reflects the difficulty of the image. We propose to use the correctly predicted patch number as the indicator of the image difficulty. This is a histogram reflecting the count of many images have a given number of patches correctly predicted the class (top right plot in Figure 9). Example images, ranging from hard on the left, to easy on the right, are shown below; the hard cases can be due either to very similar/easily confused classes or to pose-estimation failure.

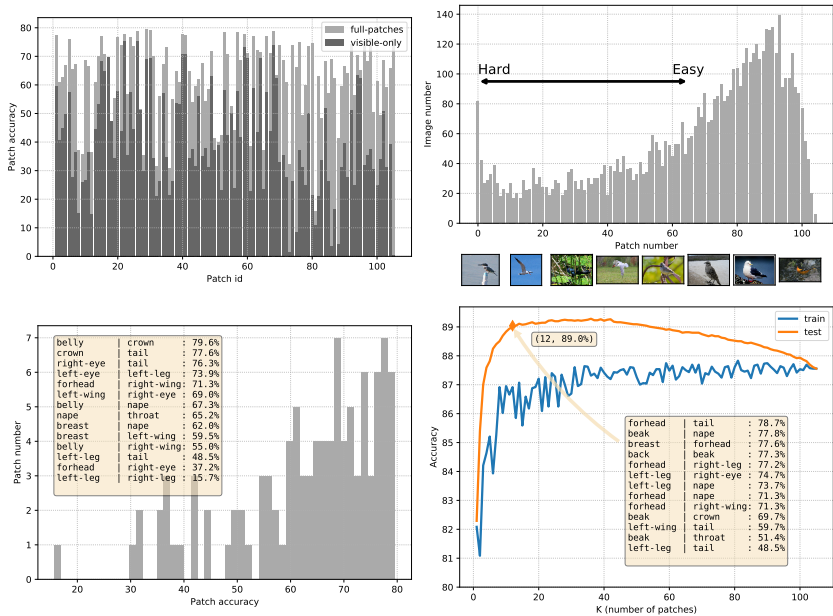


**Fig. 9. Result visualization.** Top left: we show patch classification network accuracies using two strategies, visible keypoint patch and full keypoint patch separately. This verifies that treating all keypoints as visible will help improve the patch classifier’s accuracy. Top right: hard case mining by correct prediction patch number. In the bottom we show sample images from hard to easy. Bottom left: distributions of patch classifier performance. Some examples are shown in the text box. Bottom right: Beam search results using two strategies, patch finding on training set (blue) and testing set (orange). The later one is purely for the estimation of the potential of the pair representation.

## 5 Conclusion

In this paper, we introduce the PAIRS framework, an automatic pipeline composed of keypoint detection, pose-normalized patch generalization, patch extraction, and patch score aggregation. We achieve state-of-the-art accuracy on the CUB and the NABirds datasets. Importantly, the posed-normalized patches constitute a rich object representation effective at capturing pose-aligned appearance at different scales. This simple strategy, along with the proposed pipeline, surprisingly defeats all other strongly supervised models with sophisticated attentional mechanisms. While having an end-to-end trainable network would probably further boost our performance, we argue that it is not the key for the success of our algorithm.

Finally, We’d like to draw a parallel comparison between the two seemingly unrelated tasks of fine grained recognition and object detection. As one of the most popular algorithms in object detection, two-stage detectors first locate a set of candidate objects and then classify each candidate into foreground classes or background. Similarly, our proposed pipeline first extracts pose-aligned patches and then classifies and aggregates

patch scores for final prediction. The early version of R-CNN [52], while being widely recognized as a top performing model, is also widely criticized for the model complexity and extreme slow speed. This motivates follow-on work to improving this model both performance-wise and efficiency-wise.

Although the pose-aligned patches we use in PAIRS are similar in spirit to those described in POOF [17], the POOF approach computed 5000 patches with corresponding features in order to produce the final classification, we're computing 35-70. Though not end-to-end trainable, the PAIRS model shows convincingly that part-based models, specifically pose-aligned ones, still outperform other strong baselines, and the integration of pose and appearance is a promising direction for further exploration.

## References

1. Wah, C., Branson, S., Welinder, P., Perona, P., Belongie, S.: The Caltech-UCSD Birds-200-2011 Dataset. Technical report, California Institute of Technology (2011)
2. Van Horn, G., Branson, S., Farrell, R., Haber, S., Barry, J., Ipeirotis, P., Perona, P., Belongie, S.: Building a Bird Recognition App and Large Scale Dataset With Citizen Scientists: The Fine Print in Fine-Grained Dataset Collection. In: CVPR. (2015)
3. Berg, T., Belhumeur, P.N.: How Do You Tell a Blackbird from a Crow? In: ICCV. (2013)
4. Khosla, A., Jayadevaprakash, N., Yao, B., Fei-Fei, L.: Novel dataset for Fine-Grained Image Categorization. In: CVPR Workshops (FGVC). (2011)
5. Liu, J., Kanazawa, A., Jacobs, D.W., Belhumeur, P.N.: Dog Breed Classification Using Part Localization. In: ECCV. (2012)
6. Parkhi, O.M., Vedaldi, A., Jawahar, C.V., Zisserman, A.: The truth about cats and dogs. In: ICCV. (2011)
7. Krause, J., Stark, M., Deng, J., Fei-Fei, L.: 3D Object Representations for Fine-Grained Categorization. In: ICCV Workshops (3DRR). (2013)
8. Yang, L., Luo, P., Loy, C.C., Tang, X.: A Large-Scale Car Dataset for Fine-Grained Categorization and Verification. In: CVPR. (2015)
9. Krizhevsky, A., Sutskever, I., Hinton, G.E.: Imagenet classification with deep convolutional neural networks. In Pereira, F., Burges, C.J.C., Bottou, L., Weinberger, K.Q., eds.: Advances in Neural Information Processing Systems 25. Curran Associates, Inc. (2012) 1097–1105
10. Lin, T.Y., RoyChowdhury, A., Maji, S.: Bilinear CNN Models for Fine-Grained Visual Recognition. In: ICCV. (2015)
11. Gao, Y., Beijbom, O., Zhang, N., Darrell, T.: Compact Bilinear Pooling. In: CVPR. (2016)
12. Kong, S., Fowlkes, C.C.: Low-rank Bilinear Pooling for Fine-Grained Classification. In: CVPR. (2017)
13. Huang, S., Xu, Z., Tao, D., Zhang, Y.: Part-Stacked CNN for Fine-Grained Visual Categorization. In: CVPR. (2016)
14. Zhang, N., Shelhamer, E., Gao, Y., Darrell, T.: Fine-grained pose prediction, normalization, and recognition. ICLR Workshops (2016)
15. Lin, D., Shen, X., Lu, C., Jia, J.: Deep LAC: Deep Localization, Alignment and Classification for Fine-Grained Recognition. In: CVPR. (2015)
16. Fu, J., Zheng, H., Mei, T.: Look Closer to See Better: Recurrent Attention Convolutional Neural Network for Fine-Grained Image Recognition. In: CVPR. (2017)
17. Berg, T., Belhumeur, P.N.: POOF: Part-Based One-vs.-One Features for Fine-Grained Categorization, Face Verification, and Attribute Estimation. In: CVPR. (2013)

18. Everingham, M., Eslami, S.M.A., Van Gool, L., Williams, C.K.I., Winn, J., Zisserman, A.: The pascal visual object classes challenge: A retrospective. *International Journal of Computer Vision* **111**(1) (January 2015) 98–136
19. Russakovsky, O., Deng, J., Su, H., Krause, J., Satheesh, S., Ma, S., Huang, Z., Karpathy, A., Khosla, A., Bernstein, M., Berg, A.C., Fei-Fei, L.: ImageNet Large Scale Visual Recognition Challenge. *IJCV* **115**(3) (12 2015) 211–252
20. Lin, T.Y., Maire, M., Belongie, S., Hays, J., Perona, P., Ramanan, D., Dollár, P., Zitnick, C.L.: Microsoft coco: Common objects in context. In Fleet, D., Pajdla, T., Schiele, B., Tuytelaars, T., eds.: *Computer Vision – ECCV 2014*, Cham, Springer International Publishing (2014) 740–755
21. Duan, K., Parikh, D., Crandall, D., Grauman, K.: Discovering localized attributes for fine-grained recognition. In: *CVPR*. (2012)
22. Farrell, R., Oza, O., Morariu, V.I., Zhang, N., Darrell, T., Davis, L.S.: Birdlets: Subordinate categorization using volumetric primitives and pose-normalized appearance. In: *ICCV*. (2011)
23. Yao, B., Bradski, G., Fei-Fei, L.: A codebook-free and annotation-free approach for fine-grained image categorization. In: *CVPR*. (2012)
24. Yao, B., Khosla, A., Fei-Fei, L.: Combining randomization and discrimination for fine-grained image categorization. In: *CVPR*. (2011)
25. Zhang, N., Farrell, R., Darrell, T.: Pose pooling kernels for sub-category recognition. In: *CVPR*. (2012)
26. Zhang, N., Farrell, R., Iandola, F., Darrell, T.: Deformable Part Descriptors for Fine-Grained Recognition and Attribute Prediction. In: *ICCV*. (2013)
27. Branson, S., Van Horn, G., Perona, P., Belongie, S.: Bird Species Recognition Using Pose Normalized Deep Convolutional Nets. In: *BMVC*. (2014)
28. Krause, J., Gebru, T., Deng, J., Li, L.J., Fei-Fei, L.: Learning Features and Parts for Fine-Grained Recognition. In: *ICPR*. (2014)
29. Zhang, N., Donahue, J., Girshick, R., Darrell, T.: Part-Based R-CNNs for Fine-Grained Category Detection. In: *ECCV*. (2014)
30. Lin, D., Shen, X., Lu, C., Jia, J.: Deep lac: Deep localization, alignment and classification for fine-grained recognition. In: *2015 IEEE Conference on Computer Vision and Pattern Recognition (CVPR)*. (June 2015) 1666–1674
31. Girshick, R.: Fast R-CNN. In: *CVPR*. (2015)
32. Huang, S., Xu, Z., Tao, D., Zhang, Y.: Part-stacked cnn for fine-grained visual categorization. In: *The IEEE Conference on Computer Vision and Pattern Recognition (CVPR)*. (June 2016)
33. Gavves, E., Fernando, B., Snoek, C., Smeulders, A., Tuytelaars, T.: Fine-Grained Categorization by Alignments. In: *ICCV*. (2013)
34. Gavves, E., Fernando, B., Snoek, C.G.M., Smeulders, A.W.M., Tuytelaars, T.: Local Alignments for Fine-Grained Categorization. *IJCV* **111**(2) (2015) 191–212
35. Jaderberg, M., Simonyan, K., Zisserman, A., Kavukcuoglu, K.: Spatial Transformer Networks. In: *NIPS*. (2015)
36. Cui, Y., Zhou, F., Wang, J., Liu, X., Lin, Y., Belongie, S.: Kernel Pooling for Convolutional Neural Networks. In: *CVPR*. (2017)
37. Lam, M., Mahasseni, B., Todorovic, S.: Fine-Grained Recognition as HSnet Search for Informative Image Parts. In: *CVPR*. (2017)
38. Liu, X., Wang, J., Wen, S., Ding, E., Lin, Y.: Localizing by Describing: Attribute-Guided Attention Localization for Fine-Grained Recognition. In: *AAAI*. (2017)
39. Sermanet, P., Frome, A., Real, E.: Attention for Fine-Grained Categorization. In: *ICLR*. (2015)

40. Xiao, T., Xu, Y., Yang, K., Zhang, J., Peng, Y., Zhang, Z.: The Application of Two-Level Attention Models in Deep Convolutional Neural Network for Fine-Grained Image Classification. In: CVPR. (2015)
41. Zhao, B., Wu, X., Feng, J., Peng, Q., Yan, S.: Diversified Visual Attention Networks for Fine-Grained Object Classification. *IEEE Transactions on Multimedia* **19**(6) (6 2017) 1245–1256
42. Zheng, H., Fu, J., Mei, T., Luo, J.: Learning multi-attention convolutional neural network for fine-grained image recognition. In: 2017 IEEE International Conference on Computer Vision (ICCV). (Oct 2017) 5219–5227
43. Krause, J., Sapp, B., Howard, A., Zhou, H., Toshev, A., Duerig, T., Philbin, J., Fei-Fei, L.: The Unreasonable Effectiveness of Noisy Data for Fine-Grained Recognition. In: ECCV. (2016)
44. Toshev, A., Szegedy, C.: Deeppose: Human pose estimation via deep neural networks. In: The IEEE Conference on Computer Vision and Pattern Recognition (CVPR). (June 2014)
45. Tompson, J., Jain, A., LeCun, Y., Bregler, C.: Joint training of a convolutional network and a graphical model for human pose estimation. In: Proceedings of the 27th International Conference on Neural Information Processing Systems - Volume 1. NIPS’14, Cambridge, MA, USA, MIT Press (2014) 1799–1807
46. Felzenszwalb, P.F., Girshick, R.B., McAllester, D., Ramanan, D.: Object detection with discriminatively trained part-based models. *PAMI* **32**(9) (9 2010) 1627–45
47. Shazeer, N., Mirhoseini, A., Maziarz, K., Davis, A., Le, Q.V., Hinton, G.E., Dean, J.: Outrageously Large Neural Networks: The Sparsely-Gated Mixture-of-Experts Layer. *CoRR* **abs/1701.0** (2017)
48. Krause, J., Jin, H., Yang, J., Fei-Fei, L.: Fine-Grained Recognition without Part Annotations. In: CVPR. (2015)
49. Zhang, X., Xiong, H., Zhou, W., Lin, W., Tian, Q.: Picking Deep Filter Responses for Fine-Grained Image Recognition. In: CVPR. (2016)
50. Xu, Z., Huang, S., Zhang, Y., Tao, D.: Augmenting Strong Supervision Using Web Data for Fine-Grained Categorization. In: ICCV. (2015)
51. Lin, T.Y., RoyChowdhury, A., Maji, S.: Bilinear Convolutional Neural Networks for Fine-grained Visual Recognition. *PAMI* (2018)
52. Girshick, R., Donahue, J., Darrell, T., Malik, J.: Rich Feature Hierarchies for Accurate Object Detection and Semantic Segmentation. In: CVPR. (2014)